Rigid-body rotation of an electron cloud in divergent magnetic fields

A. Fruchtman, R. Gueroult, and N. J. Fisch

Citation: Phys. Plasmas **20**, 073502 (2013); doi: 10.1063/1.4813243
View online: http://dx.doi.org/10.1063/1.4813243
View Table of Contents: http://pop.aip.org/resource/1/PHPAEN/v20/i7
Published by the AIP Publishing LLC.

Rigid-body rotation of an electron cloud in divergent magnetic fields

A. Fruchtman,[1] R. Gueroult,[2] and N. J. Fisch[2]
[1]*H.I.T.—Holon Institute of Technology, Holon 58102, Israel*
[2]*Princeton Plasma Physics Laboratory, Princeton University, New Jersey 08543, USA*

(Received 29 March 2013; accepted 4 June 2013; published online 10 July 2013)

For a given voltage across a divergent poloidal magnetic field, two electric potential distributions, each supported by a rigid-rotor electron cloud rotating with a different frequency, are found analytically. The two rotation frequencies correspond to the slow and fast rotation frequencies known in uniform plasma. Due to the centrifugal force, the equipotential surfaces, that correspond to the two electric potential distributions, diverge more than the magnetic surfaces do, the equipotential surfaces in the fast mode diverge largely in particular. The departure of the equipotential surfaces from the magnetic field surfaces may have a significant focusing effect on the ions accelerated by the electric field. The focusing effect could be important for laboratory plasma accelerators as well as for collimation of astrophysical jets. © *2013 AIP Publishing LLC*. [http://dx.doi.org/10.1063/1.4813243]

I. INTRODUCTION

Because of the high mobility of electrons along magnetic field lines, it is often assumed that the potential over a magnetic flux surface is constant. Indeed, the assumption that magnetic surfaces tend also to be equipotential surfaces has been utilized in the design of the potential distribution in many magnetic devices, including the Hall thruster,[1] plasma lens,[2,3] tandem mirror,[4] centrifugal fusion,[5–7] plasma centrifuge,[8–10] or helicon source.[11,12] We have recently shown that in fact, because of the centrifugal force, equipotential surfaces do not coincide with magnetic flux surfaces and that this inclination of the equipotential surface with respect to the magnetic surfaces may have focusing effect on ion beams.[13] In this paper, we examine the electric potential distribution in an electron cloud immersed in a divergent poloidal magnetic field.

A divergent poloidal magnetic field with a large axial component is characteristic to the cylindrical Hall thruster (CHT).[14] The CHT is a promising alternative to the conventional annular Hall Thruster. A number of variations of Hall thrusters with large axial field components, similar to the CHT, have now been explored as well.[15–18] In this open or magnetic-nozzle configuration, the outer part of the central portion of a conventional HT annular channel is eliminated, giving a larger volume to surface ratio for a given thruster radial dimension, resulting in smaller electron losses to the walls and therefore a smaller erosion. A result of the elimination of that central portion is a significantly larger component of the magnetic field in the axial direction compared to the magnetic field in the conventional annular Hall thruster. Thus, while there are many magnetic field effects such as magnetic mirroring or focusing exhibited by the conventional annular thruster,[17–21] we are interested here in magnetic field configurations with a large axial component.

The potential distributions across the magnetic flux surfaces in the CHT determine the ion dynamics. We were able to find and to describe analytically two electric potential distributions, each supported by a rigid-rotor electron cloud rotating with a different frequency. The two rotation frequencies correspond to the slow and fast rotation frequencies known in uniform plasma.[22] Due to the centrifugal force, both equipotential surfaces that correspond to the two electric potential distributions, diverge more than the magnetic surfaces do, the potential in the fast mode deviates largely in particular. The departure of the equipotential surfaces from the magnetic field surfaces may have a significant effect on the divergence of an ion beam accelerated by the electric field. We show that the larger divergence of the equipotential surfaces has a nonmonotonic effect on the direction of accelerated ions, although, in general, a considerable focusing effect is expected. In addition to the CHT, the focusing effect could be important for other laboratory plasma accelerators as well as for collimation of astrophysical jets.[23]

In Sec. II, we present the two families of equipotential surface with the corresponding two rotating electron clouds. In Sec. III, we demonstrate the effect of the deviation of the equipotential surfaces from the magnetic surfaces on the dynamics of unmagnetized ions that are accelerated by the electric field.

II. EQUIPOTENTIAL SURFACES IN THE PRESENCE OF ROTATING ELECTRON CLOUDS

We assume that there is a force balance on the electrons and neglect electron inertia terms except the centrifugal force term

$$\vec{E} + v_\vartheta \hat{\vartheta} \times \vec{B} = \frac{m}{e}\frac{v_\vartheta^2}{r}\hat{r}. \tag{1}$$

Here, $\vec{E}$ and $\vec{B}$ are the electric and magnetic fields, v_ϑ is the azimuthal component of the electron fluid velocity, m is the electron mass, and e is the elementary charge. In Eq. (1), the component of $\vec{E}$ parallel to $\vec{B}$ is balanced by the component of the centrifugal force parallel to $\vec{B}$. If there is no centrifugal force, $\vec{E}$ parallel to $\vec{B}$ is zero, and the electric potential is constant along a field line. We are examining here the effect of a finite centrifugal force.

We note that the electrons have thermal velocity with components in both the r and the z directions. In addition, there is a drift velocity towards the anode. However, we assume that, due to the large applied electric field, the largest component of the velocity is in the azimuthal direction. To lowest order, we retain only that component in Eq. (1).

We use cylindrical coordinates assuming that there is only a poloidal field, $\vec{B} = (B_z, B_r, 0)$, and that there is no variation in the ϑ direction. The fields are expressed with the magnetic flux function ψ and the electric potential ϕ as

$$\vec{B} = \vec{\nabla} \times \left(\hat{\vartheta} \frac{\psi}{r} \right), \quad \vec{E} = -\vec{\nabla}\phi. \tag{2}$$

From the z and r components of Eq. (1), we derive the governing equation

$$-\frac{\partial\phi}{\partial r^2}\frac{\partial\psi}{\partial z} + \frac{\partial\phi}{\partial z}\frac{\partial\psi}{\partial r^2} = \frac{m}{2e}\frac{(\partial\phi/\partial z)^2}{\partial\psi/\partial z}. \tag{3}$$

The effect of the centrifugal force is obvious also from Eq. (3). If the centrifugal force is neglected so that the right hand side (RHS) of the equation is zero, ψ and ϕ commute resulting in the coinciding of the equipotential surfaces and the magnetic flux surfaces. We are interested in the more general case, when the centrifugal force is not zero, so that these two families of surfaces do not coincide. Our approach is to take $\psi(z,r)$ as given and to solve for $\phi(z,r)$ for a divergent magnetic field. We use a magnetic flux function of the form[24] $\psi = (B_0/2)r^2/[(1 + r/R)^2 + z^2/R^2]^{3/2}$. Since in the present paper we address the case of a magnetic field with a large axial component, we use the paraxial approximation and approximate further to

$$\psi = \frac{B_0 r^2}{2(1 + z^2/R^2)^{3/2}}. \tag{4}$$

The magnetic field associated with ψ of Eq. (4) is not curl-free, and the associated azimuthal current density is on the order of $B_0 r/R^2\mu_0$, usually smaller than the actual azimuthal current in the CHT, which induces a small perturbation only to the vacuum field. In any event, our aim is to demonstrate the deviation of the equipotential surfaces from the magnetic flux surfaces for a prototypical case of a diverging magnetic field, and the exact form of the magnetic field surfaces is not that important.

We look for $\phi(z,r)$ that satisfies Eq. (3) when the electric potential $\phi(z=0,r)$ is specified as follows:

$$\phi(z=0,r) = \phi_1 \frac{r^2}{r_1^2}, \quad 0 \le r \le r_1. \tag{5}$$

Without the centrifugal force, the curves of constant ψ are the characteristics of the equation for ϕ and the potential distribution is simply

$$\phi(z,r) = \phi_1 \frac{r^2}{r_1^2}\frac{1}{(1 + z^2/R^2)^{3/2}}. \tag{6}$$

Taking into account the centrifugal force, we seek a solution of the form $\phi(z,r) = \phi_1 \varsigma g(f)$, where $\varsigma \equiv r^2/r_1^2$ and $f \equiv 1/(1 + z^2/R^2)^{3/2}$. The governing equation (3) with the magnetic flux of the form (4) becomes

$$pg'^2 - fg' + g = 0, \tag{7}$$

where according to the boundary condition (5), $g(1) = 1$, and

$$p \equiv \frac{2m\phi_1}{eB_0^2 r_1^2}. \tag{8}$$

Here, $g' \equiv dg/df$. Substituting $u \equiv g(f)/f^2$ and $s = \ln f$ into Eq. (7), we obtain the nonlinear homogeneous differential equation: $p(2u + du/ds)^2 - (2u + du/ds) + u = 0$. This equation is easily integrated to provide two analytical solutions to Eq. (3) with the boundary condition (5)

$$\phi(z,r) = \frac{\phi_1 r^2}{4pr_1^2}\left(1 \mp \sqrt{1-4p}\right) \times \left[\frac{2}{(1 + z^2/R^2)^{3/2}} - \left(1 \mp \sqrt{1-4p}\right)\right]. \tag{9}$$

The two solutions correspond to the two rotation modes known in uniform plasma,[22] the slow mode and the fast mode (upper and lower sign, respectively). Calculating the rotational frequency as $\Omega = v_\vartheta/r = (\partial\phi/\partial z)/(\partial\psi/\partial z)$, we find that

$$\Omega = \frac{eB_0}{2m}\left(1 \mp \sqrt{1-4p}\right), \tag{10}$$

which are the two frequencies in a uniform magnetic field[22] calculated at $z = 0$. The two rigid-rotor equilibria coincide at the Brillouin flow, when $4p = 1$. At the limit $p \to 0$, the slow mode of Eq. (9) is reduced to that in Eq. (6).

The parameter p can also be expressed as $(E/rB)/\Omega_c$, where Ω_c is the electron cyclotron frequency and the quantities are taken at $z = 0$.

We note on passing that, when $4p = 1$, Eq. (7) has a third solution, $u = 1$ or $g = f^2$, which is written explicitly as

$$\phi(z,r) = \phi_1 \frac{r^2}{r_1^2}\frac{1}{(1 + z^2/R^2)^3}. \tag{11}$$

This additional solution for $4p = 1$ is different from the two rotation modes described above. It is a special case of a particular solution for Eq. (3)

$$\phi(z,r) = \frac{e}{2m}\left(\frac{\psi}{r}\right)^2. \tag{12}$$

The electric potential described by Eq. (12) satisfies the governing equation (3) for any magnetic flux function, ψ, not only for ψ of the form (4). The rotational frequency in the case of the particular solution is found again through $\Omega = v_\vartheta/r = (\partial\phi/\partial z)/(\partial\psi/\partial z)$ with $4p = 1$

$$\Omega = \frac{eB_0}{2m}\frac{1}{(1 + z^2/R^2)^{3/2}}. \tag{13}$$

This is a rigid-rotor equilibrium but the rotational frequency varies along z. This variation implies that the flow is not iso-rotational.

We turn back to the rigid-rotor flows [Eqs. (9) and (10)]. The equipotential surfaces determined by Eq. (9) do not coincide with the magnetic field surfaces. The equipotential surfaces of the slow mode equilibrium do converge to the magnetic field surfaces at the limit $p \to 0$. In the fast mode, however, the deviation of the equipotential surfaces becomes larger as $p \to 0$. That deviation of the fast mode may have a dramatic effect on ion beam collimation.

Figures 1 and 2 show the magnetic flux surfaces and the equipotential surfaces according to Eq. (9) for $r_1/R = 0.1$. Figure 1 shows these surfaces for the Brillouin limit at $4p = 1$, for which $\Omega = eB_0/2m$ for the two rotational modes. Figure 2 shows the equipotential surfaces for the two modes for $p = 0.2$. While the deviation of the equipotential surfaces from magnetic flux surfaces is small for the slow mode, that deviation is very large for the fast mode.

III. THE ION DYNAMICS

We solve for ion trajectories under magnetic fields and electric fields derived from the magnetic flux function (4) and electric potential (9). We assume that the potential distribution corresponds to the slow mode, which we write in the form

$$\phi(z,r) = \frac{\phi_1 r^2}{4pr_1^2}\left(1-\sqrt{1-4p}\right) \times \left[\frac{2}{(1+z^2/R^2)^{3/2}} - \left(1-\sqrt{1-4p}\right)\right]. \quad (14)$$

We write the equation of motion for the ions in the following dimensionless form:

$$\frac{d^2(\vec{r}/R)}{d\tau^2} = \vec{a} + \sqrt{\frac{m}{m_i}}\frac{d(\vec{r}/R)}{d\tau} \times \vec{b}, \quad (15)$$

where m_i is the ion mass, and τ, $\vec{a}$, and $\vec{b}$, the normalized time, electric field, and magnetic field, are

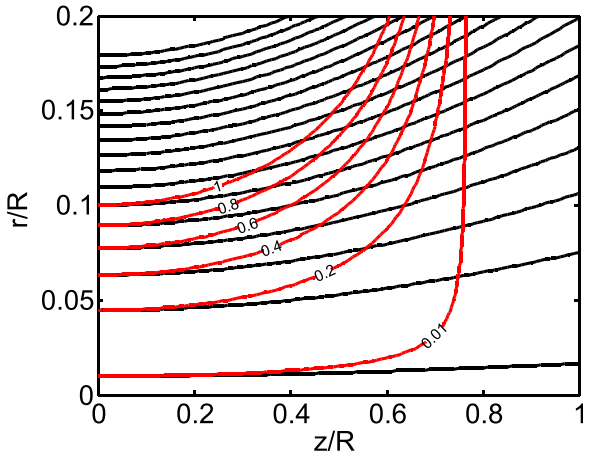

FIG. 1. Normalized magnetic flux surfaces $2\psi/B_0r_1^2$ and normalized equipotential surfaces ϕ/ϕ_1 (colored)-Brillouin flow–$4p = 1$.

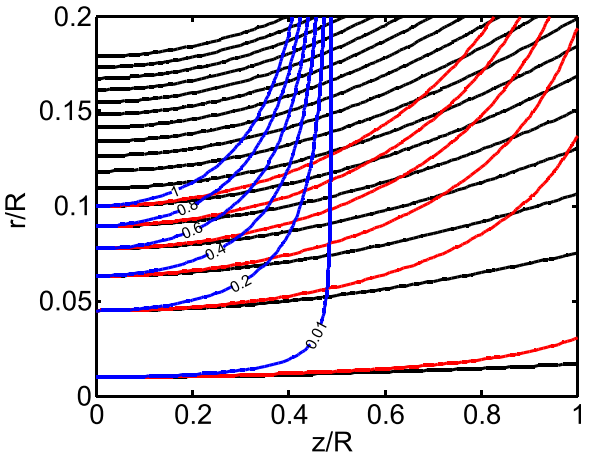

FIG. 2. Normalized magnetic flux surfaces $2\psi/B_0r_1^2$ and normalized equipotential surfaces ϕ/ϕ_1 for the slow mode (red) and for the fast mode (blue)–$p = 0.2$.

$$\tau \equiv \frac{eB_0}{\sqrt{mm_i}}t, \quad \vec{a}(p,r/R,z/R) \equiv m/eB_0^2R\vec{E},$$
$$\vec{b}(r/R,z/R) \equiv \frac{\vec{B}}{B_0}. \quad (16)$$

A diagram of the cylindrical Hall thruster, for which this analysis is relevant, is shown in Fig. 3. Our solution for the electric potential holds in the bulk of the plasma. We do not address the problem of matching our solution to the solution at the plasma plume outside the magnetized region. There a different model has to be used. However, it stands to reason that at a certain distance from the axis on the plane denoted as $z = 0$, the potential is close to that at the anode, $\phi = \phi_1$, while on axis the potential is that of the cathode, which we denote as $\phi = 0$. It is likely that the potential drops to the cathode potential at some plane in the vicinity of the

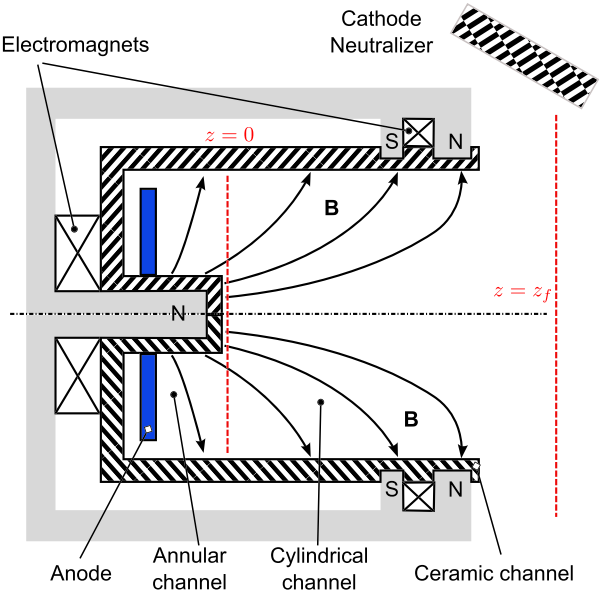

FIG. 3. A schematic of the cylindrical Hall thruster. As an illustration, denoted are planes $z = 0$ and $z = z_f$ that correspond to the particular analytical solution.

cathode, there $\phi = 0$. Somewhat arbitrarily, we assume that this plane is perpendicular to the axis of symmetry, and according to Eq. (14) it satisfies

$$\frac{2}{(1+z_f^2/R^2)^{3/2}} - \left(1-\sqrt{1-4p}\right) = 0 \tag{17}$$

so that $\phi = 0$ at all r. A plane denoted as $z = z_f$ is shown in Fig. 3.

If an ion is released at rest at any $r \le r_1$, at the plane $z = 0$, it will only oscillate around $r = 0$, without moving axially. We solve the equations of motion under the assumption that an ion is released at rest at $z = z_i > 0$ at $\phi(z_i, r_i) = \phi_1$, so that r_i satisfies

$$1 = \frac{r_i^2}{4pr_1^2}\left(1-\sqrt{1-4p}\right)\left[\frac{2}{(1+z_i^2/R^2)^{3/2}} - \left(1-\sqrt{1-4p}\right)\right]. \tag{18}$$

We examine what the velocity of the ion is as it propagates through the exit at z_f, as described above.

If the centrifugal force is neglected, the electric potential becomes

$$\phi(z,r) = \frac{\phi_1 r^2}{r_1^2(1+z^2/R^2)^{3/2}}, \tag{19}$$

as is obtained at the limit $p \to 0$ [see Eq. (6)]. For each initial location (z_i, r_i), we compare an ion trajectory in the presence of the potential of the slow mode, as in Eq. (14), due to the centrifugal force, with an ion trajectory in the absence of the centrifugal force, the slab case, as in Eq. (19). Note that in the slab case the potential ϕ vanishes at a different, curved plane.

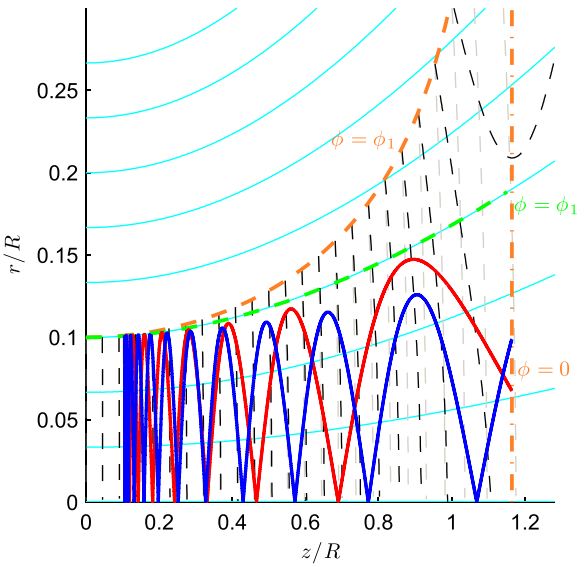

FIG. 4. Ion trajectories under the magnetic field and the electric field that corresponds to the slow mode for $p = 0.2$ (red), and in the slab case $p \to 0$ (blue), both for $z_i/R = 0.1$. The angle of divergence at the exit is 21° and 39°, respectively. Also shown are the magnetic field lines, and the electric field lines for the slow mode (black dashed) and for the slab case (gray dashed), the $\phi = \phi_1$ (orange dashed) and $\phi = 0$ (orange dotted-dashed) lines for the slow mode and the $\phi = \phi_1$ (green dashed) for the slab case.

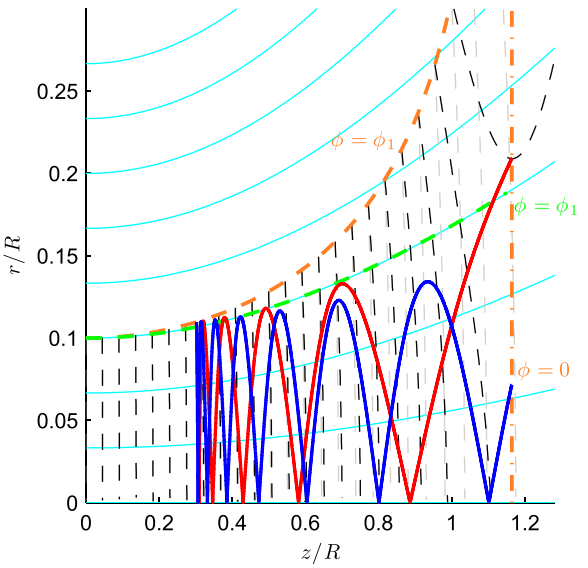

FIG. 5. Ion trajectories under the same magnetic and electric fields as in Fig. 4. Here, $z_i/R = 0.3$. The angle of divergence at the exit is 26° for the slow mode and 46° for the slab case.

In Figs. 4–7, we show the results for the initial conditions $z_i/R = 0.1, 0.3, 0.7$, and 0.9, respectively. The parameters in the calculations are $r_1/R = 0.1$ as in Figs. 1 and 2 (which determines the values of r_i/R), and $m/m_i = 1.36 \times 10^{-5}$ (corresponding to argon). For the case with the centrifugal force, $p = 0.2$, while for the slab case, $p \to 0$. In the comparison, we chose to compare in each of Figs. 4–7 the trajectories of ions that are born at the same location. Since the equipotential surfaces are different when the centrifugal force is different, the ion trajectories compared in each figure are accelerated across different voltages.

Because of the ion oscillations around the axis, the angle of the ion motion at the exit is hardly predictable. The angle of the ion trajectory is sometimes smaller with the centrifugal force and sometimes larger. For example, when

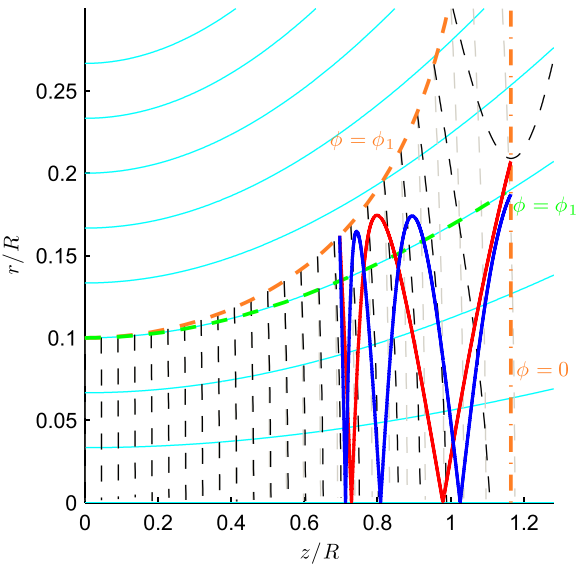

FIG. 6. Ion trajectories under the same magnetic and electric fields as in Fig. 4. Here, $z_i/R = 0.7$. The angle of divergence at the exit is 42° for the slow mode and 24° for the slab case.

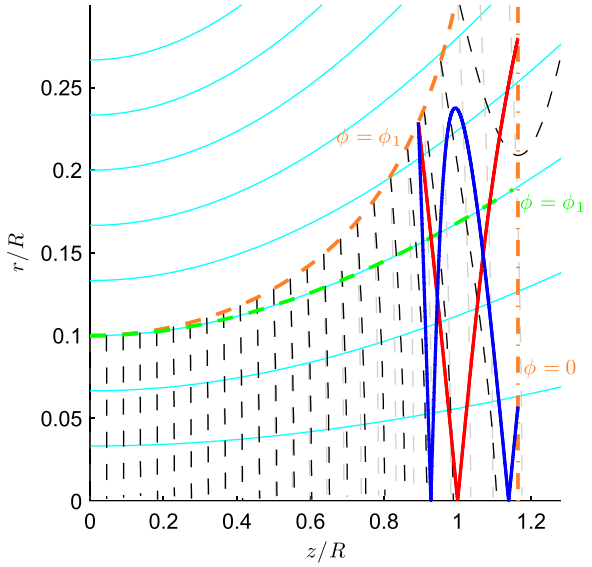

FIG. 7. Ion trajectories under the same magnetic and electric fields as in Fig. 4. Here, $z_i/R = 0.9$. The angle of divergence at the exit is 46° for the slow mode and 66° for the slab case.

$z_i/R = 0.7$ (Fig. 6), the angle at the exit is 42° with the centrifugal force, and it is only 24° in the slab case.

Ions that are borne near the exit leave the system with the centrifugal force without bouncing off the axis. Such trajectories are not shown here. However, it is clear that in that region the angle of the ion trajectory relative to the axis is smaller with the centrifugal force. We note that the trajectories we show are of ions that were born near the axis, because our calculation is for a magnetic field that is described within the paraxial approximation. The relative number of ions that leave the system without bouncing off axis is expected to be larger if they are born away from the axis. Because the number of ions that do not bounce off axis

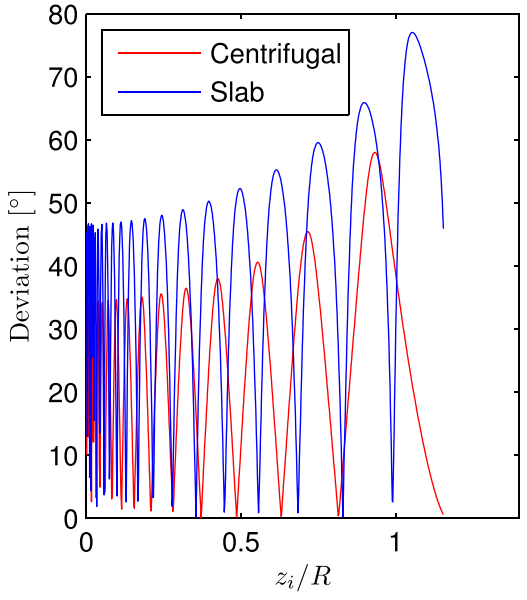

FIG. 8. The angle of divergence of the ions at the exit versus z_i/R under the electric field that corresponds to the slow mode (red), $p = 0.2$, and in the slab case (blue). The average angles of divergence for the slow mode and in the slab case (over the whole z_i/R values) are, respectively, 25° and 42°.

is expected to be larger in experiments than in the region in our calculation, the effect of the centrifugal force on reducing the angle of divergence is also expected to be larger than what is shown in the figures here.

Figure 8 shows the angle of divergence of the ions at the exit versus z_i/R under the electric field as in Figs. 4–7. The average angle of divergence, over all values of z_i/R in Fig. 8, is 25° in the presence of the centrifugal force ($p = 0.2$), while in the slab case ($p \to 0$) the average angle is 42°. Thus, the results confirm our prediction[13] of the focusing effect of the centrifugal force.

IV. SUMMARY

We have described analytically two electric potential distributions, each supported by a rigid-rotor electron cloud rotating with a different frequency, across a divergent poloidal magnetic field. These potential distributions and the associated rotation frequencies correspond to the slow and fast rotation frequencies known in uniform plasma. The centrifugal force on the rotating clouds is the source of the two steady-state distributions.

We have shown that, due to the centrifugal force, the equipotential surfaces, which correspond to the two electric potential distributions, diverge more than the magnetic surfaces do; the divergence is particularly large for equipotential surfaces in the fast mode. The departure of the equipotential surfaces from the magnetic field surfaces may have a significant focusing effect on the ions accelerated by the electric field. That focusing effect has been examined here for the slow mode by calculating ion trajectories in the specified magnetic and electric fields. The numerical solutions confirm our previous prediction[13] and show that, indeed, the divergence of equipotential surfaces due to the centrifugal force has a collimating effect on the exiting ion beam.

It remains to find efficient means of exciting the fast mode that was described here. In addition, for a specified potential along a plane, we found two (and sometimes even three) different electric potential distributions in the same domain. It also remains to explore what physical boundary conditions could allow a unique solution. It remains as well to explore how the focusing, that results from the deviation of the equipotential surfaces from the magnetic flux surfaces, affects laboratory plasma accelerators, such as the cylindrical Hall thruster, and, perhaps, the collimation of astrophysical jets.

ACKNOWLEDGMENTS

This work was partially supported by the US–Israel Binational Science Foundation under Grant No. 2008224. R.G. and N.J.F. acknowledge support by US DOE under Contract Nos. DE-FG02-06ER54851 and DEAC02-09CH11466.

[1]A. I. Morozov and V. V. Savelyev, "Fundamentals of stationary plasma thruster theory," in *Reviews of Plasma Physics*, edited by B. B. Kadomtsev and V. D. Shafranov (Consultants Bureau, New York, 2000), Vol. 21.
[2]A. I. Morozov, Plasma Phys. Rep. **29**, 235 (2003).

[3]A. A. Goncharov, A. N. Evsyukov, and I. V. Litovko, IEEE Trans. Plasma Sci. **37**, 1283 (2009).
[4]G. D. Severn and N. Hershkowitz, Phys. Fluids B **4**, 3210 (1992).
[5]B. Lehnert, Nucl. Fusion **11**, 485 (1971).
[6]Y. M. Huang and A. B. Hassam, Phys. Rev. Lett. **87**, 235002 (2001).
[7]V. I. Volosov, Nucl. Fusion **46**, 820 (2006).
[8]A. J. Fetterman and N. J. Fisch, Phys. Rev. Lett. **101**, 205003 (2008).
[9]M. Krishnan, M. Geva, and J. L. Hirshfield, Phys. Rev. Lett. **46**, 36 (1981).
[10]T. Ohkawa and R. Miller, Phys. Plasmas **9**, 5116 (2002).
[11]A. V. Arefiev and B. N. Breizman, Phys. Plasmas **12**, 043504 (2005).
[12]T. Lafleur, K. Takahashi, C. Charles, and R. W. Boswell, Phys. Plasmas **18**, 080701 (2011).
[13]N. J. Fisch, Y. Raitses, and A. Fruchtman, Plasma Phys. Controlled Fusion **53**, 124038 (2011).
[14]Y. Raitses and N. J. Fisch, Phys. Plasmas **8**, 2579 (2001).
[15]A. Shirasaki and H. Tahara, J. Appl. Phys. **101**, 073307 (2007).
[16]N. A. MacDonald, M. A. Cappelli, S. R. Gildea, M. Martinez-Sanchez, and W. A. Hargus, Jr., J. Phys. D: Appl. Phys. **44**, 295203 (2011).
[17]R. R. Hofer, R. S. Jankovsky, and A. D. Gallimore, J. Propul. Power **22**, 721 (2006).
[18]J. A. Linnell and A. D. Gallimore, Phys. Plasmas **13**, 103504 (2006).
[19]M. Keidar and I. D. Boyd, Appl. Phys. Lett. **87**, 121501 (2005).
[20]A. Fruchtman and A. Cohen-Zur, Appl. Phys. Lett. **89**, 111501 (2006).
[21]E. Fossum and L. King, IEEE Trans. Plasma Sci. **36**, 2088 (2008).
[22]R. C. Davidson, *Theory of Nonneutral Plasmas* (Addison-Wesley, Redwood City, 1989).
[23]C. Fendt, Astrophys. J. **651**, 272–287 (2006).
[24]P. F. Schmit and N. J. Fisch, J. Plasma Phys. **75**, 359 (2009).